JOURNAL OF MATERIALS SCIENCE **35** (2000) 1661–1667

The erosion of H21 tool steel in molten A380 alloy

M. YAN, Z. FAN
Department of Materials Engineering, Brunel University, Uxbridge, Middlesex UB8 3PH, UK
E-mail: mtstzzf@brunel.ac.uk

The chemical interaction between H21 tool steel and molten A380 alloy was investigated at 700°C under dynamic conditions. Cr_2O_3-coated H21 samples were also investigated under the same condition for comparison. Samples were rotated at 300 rpm. The test time was varied between 1 and 36 hours. The reaction zone was characterised by SEM and EDS analysis. It was found that, from A380 alloy to H21 steel, $FeAl_3$, Fe_2Al_5 and $FeAl_2$ intermetallic compounds formed in sequence. Major alloying elements from both H21 steel and A380 alloy were present in those intermetallic compounds. $FeAl_3$ compound was porous, while Fe_2Al_5 and $FeAl_2$ compounds were compact. The thickness of Fe_2Al_5 layer kept constant in the range of 7–10 μm during the tests, while the thickness of $FeAl_3$ and $FeAl_2$ compounds increased with increasing test time. Under the dynamic conditions, the high erosion rate of H21 sample in molten A380 alloy may be attributed to dissolution, swift melt agitation and poor protective effect of the reaction zone. It was also found that although Cr_2O_3-coating could protect H21 steel to some extent from erosion in molten A380 alloy, it can only act as a diffusion barrier because the coating itself was attacked by molten Al-alloy through chemical dissolution.

1. Introduction

The interaction of iron-based alloys, including steels and cast irons, with liquid aluminium is of considerable importance to engineering applications, such as containment of liquid aluminium and fabrication of casting equipment. In the service conditions of pressure die casting, liquid aluminium alloy fills the die cavity at a high velocity, leading to the erosion of die walls. In semi-solid processing, the rapid relative motion of the semi-solid metal to the stationary components can lead to severe erosion to the processing equipment. Material loss resulted from erosion gives rise to the premature failure of dies and containers, as well as the degradation of casting precision.

In the literature, investigations on the chemical interaction between iron-base alloys and liquid aluminium were conducted from several to thousands of minutes, but generally less than 1 hour. Basic understanding of such interaction has been established. The interaction was usually controlled by diffusion after initial reaction stage of a very short period of time. Usually two intermetallic layers were identified in the reaction zone, namely, $FeAl_3$ next to aluminium alloy and Fe_2Al_5 next to steel [1–6]. $FeAl_2$ was also observed in H13 steel submerged in liquid A380 alloy [7]. An common feature observed in such investigations was that protuberances were formed at the outer layer of the reaction zone, extending into the liquid aluminium [7–9]. Its breaking-off into the aluminium was deemed a factor of significance to the erosion rate of steel.

So far there have been few reports on long-term interaction. However the understanding for long-term Fe/Al reaction as well as data on material loss rate, is also of importance for technological applications. In this paper, we report our work on interaction of H21 tool steel with liquid A380 alloy in the time range between 1 and 36 hours under dynamic conditions. In addition, the effect of Cr_2O_3 coating on the erosion rate of H21 steel was also investigated.

2. Experiment

The experimental apparatus used for erosion tests is illustrated schematically in Fig. 1. The erosion experiment was conducted by rotating a cylindrical H21 steel specimen around its axis in molten aluminium alloy. The rotating system was driven by a variable speed DC motor. The rotating speed can be varied between 50–1000 rpm with a controlling accuracy of ±5 rpm. Test specimen was fixed in a water-cooled sample holder to minimise the heat transferred to the drive motor. Precautions were taken to ensure the alignment along the rotation axis. The temperature of aluminium melt was measured by a chromel-alumel thermocouple with an accuracy of ±2°C. Al-alloy was contained in an alumina crucible. Melting was conducted in a resistance furnace with a reasonably good temperature control. The drive system, melting system and water-cooling system were centrally controlled through a control panel. For all the test runs the erosion temperature was kept at 700°C, and the rotation speed was 300 rpm. The erosion time was varied between 1 and 36 hours. The major experimental parameters are summarised in Table I.

The composition limit of H21 steel sample was 8.50–10.0% W, 3.00–3.75% Cr, 0.30–0.60% V, 0.15–0.40% Mn, 0.26–0.36% C, 0.15–0.50% Si, less than

TABLE I Summary of the experimental parameters of the erosion tests

Sample material	Diameter (mm)	Temperature (°C)	Rotating speed (rpm)	Test time (hour)
Uncoated H21	10	700	300	1 4 9 16 —
Coated H21	10.1	700	300	1 4 9 16 36

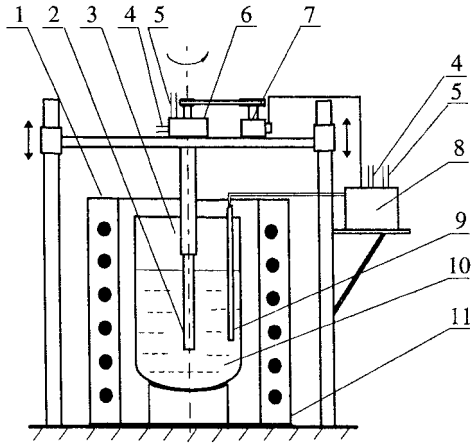

Figure 1 Schematic diagram of the experimental apparatus. 1: furnace cover; 2: sample; 3: sample holder; 4: water in; 5: water out; 6: gear box; 7: motor; 8: control panel; 9: thermocouple; 10: Al-alloy melt; 11: resistance furnace.

0.30% Ni, and balanced Fe. The selected aluminium alloy was A380. Its normal composition was 8% Si, 3.5% Cu, less than 0.3% Mg and balanced Al. Two groups of samples, coated and uncoated with chromium oxide, were tested. In both groups the H21 samples were 10 mm in diameter and 100 mm in length. In the coated group the coating was produced by plasma spray method at Plasma Coatings Ltd (Tidsswell, UK). The final thickness of coating was polished to 50 μm, giving rise to a diameter increment of 0.1 mm.

When the molten Al-alloy in the crucible reached a steady temperature of 700°C, the rotating system was started and H21 sample was lowered into the molten alloy once the rotation speed was stabilised at 300 rpm. The rotating sample was immersed deep into the melt to make sure that the erosion of a large part of sample was not affected by the oxide layer on the melt surface. After a predetermined erosion time, the sample was raised from the crucible and cooled in air. Specimens for microscopic observations were cut from the near-bottom part of the sample, normal to its axis. Measurement of the remained sample diameter excluding the reaction zone was carried out microscopically to determine the erosion loss. Each datum was an average of at least 5 measurements. Optical microscopy, scan electron microscopy (SEM), and electron dispersion spectrum (EDS) were used to characterise the reaction zone between H21 steel and A380 alloy. In addition, microhardness measurement was conducted in different intermetallic phases of interest. Every datum was the common value of over 10 points.

For coated samples similar microscopic investigation and analysis were also conducted to characterise the interfaces of Cr_2O_3 coating with A380 and H21 steel.

3. Experimental results

3.1. Uncoated samples

The morphology of the reaction zone between H21 steel and molten A380 alloy is presented in Fig. 2 as a function of erosion time. In all the SEM micrographs in Fig. 2, H21 steel is located at the left-hand side and A380 alloy at the right-hand side. As shown in Fig. 2a, two different reaction layers were formed after 1 hour test. One was thin and compact, and the other was thick and porous. The thin layer with a thickness of 8–10 μm was formed next to H21 steel. Taking the concentration of iron, chromium and manganese into account, quantitative EDS analysis indicated that this layer was Fe_2Al_5 compound. In the compound iron atoms was partially replaced by chromium and manganese, giving rise to a compound of $(Fe, Cr, Mn)_2Al_5$. For simplicity, $(Fe, Cr, Mn)_2Al_5$ will be referred as Fe_2Al_5 hereafter. The porous thick layer, with a thickness of typical 120 μm, was formed next to aluminium alloy. EDS results revealed the composition of this layer was (Fe, Cr, Mn)Al_3 intermetallic compound, which will be referred as $FeAl_3$ compound in this paper. In both compounds silicon was also detected. Similarly, after 4-hour test only Fe_2Al_5 and $FeAl_3$ phases were observed, as shown in Fig. 2b. The thickness of the porous $FeAl_3$ layer grew to 135–148 μm, while the thickness of Fe_2Al_5 layer remained almost unchanged, 8–10 μm.

After 9-hour test the variation in thickness of the reaction zone became more announced around the periphery of the sample. H21 steel was attacked less at places where the reaction zone was thicker. A new layer of intermetallic compound was observed in addition to Fe_2Al_5 and $FeAl_3$, as shown in Fig. 2c to e. The new layer, as labelled "1" in Fig. 2c, was situated between H21 steel and Fe_2Al_5 layer. Fig. 2d is a secondary electron image of Fig. 2c. A comparison between Fig. 2c and d gave more characteristics of the interfacial morphology. The new layer with a thickness of 20–49 μm was compact and was identified as (Fe, Cr, Mn)Al_2 compound by EDS analysis, and will be referred as $FeAl_2$ hereafter. The porous $FeAl_3$ layer, grew to 194–412 μm thick after 9-hour test. In this layer the porosity level was significantly higher in the region next to aluminium alloy (as labelled layer "3_b" in Fig. 2c) than in the region away from aluminium alloy (as labelled "3_a" in Fig. 2c). Fe_2Al_5 layer (labelled as "2" in Fig. 2c) was between the $FeAl_2$ and $FeAl_3$ layers. Fig. 2e was a higher magnification of the reaction zone in Fig. 2c. The thickness of Fe_2Al_5 layer remained 8–10 μm. Its interface was straight with $FeAl_2$ layer, and uneven with $FeAl_3$ layer. The aluminium melt was labelled as "4" in Fig. 2c. The morphology of the reaction zone after 16-hour test was shown in Fig. 2f. The thickness of $FeAl_3$ layer became 458–960 μm, and that of $FeAl_2$ layer 80–160 μm. It was interesting to note that the thickness of Fe_2Al_5 compound still remained constant. The thickness of intermetallic layers after different erosion time is listed in Table II.

It was observed that the interface between $FeAl_3$ compound and A380 melt was kept primarily straight throughout the test, no protuberance was observed in our experiment. Both $FeAl_2$ and $FeAl_3$ compounds grew thicker with erosion time.

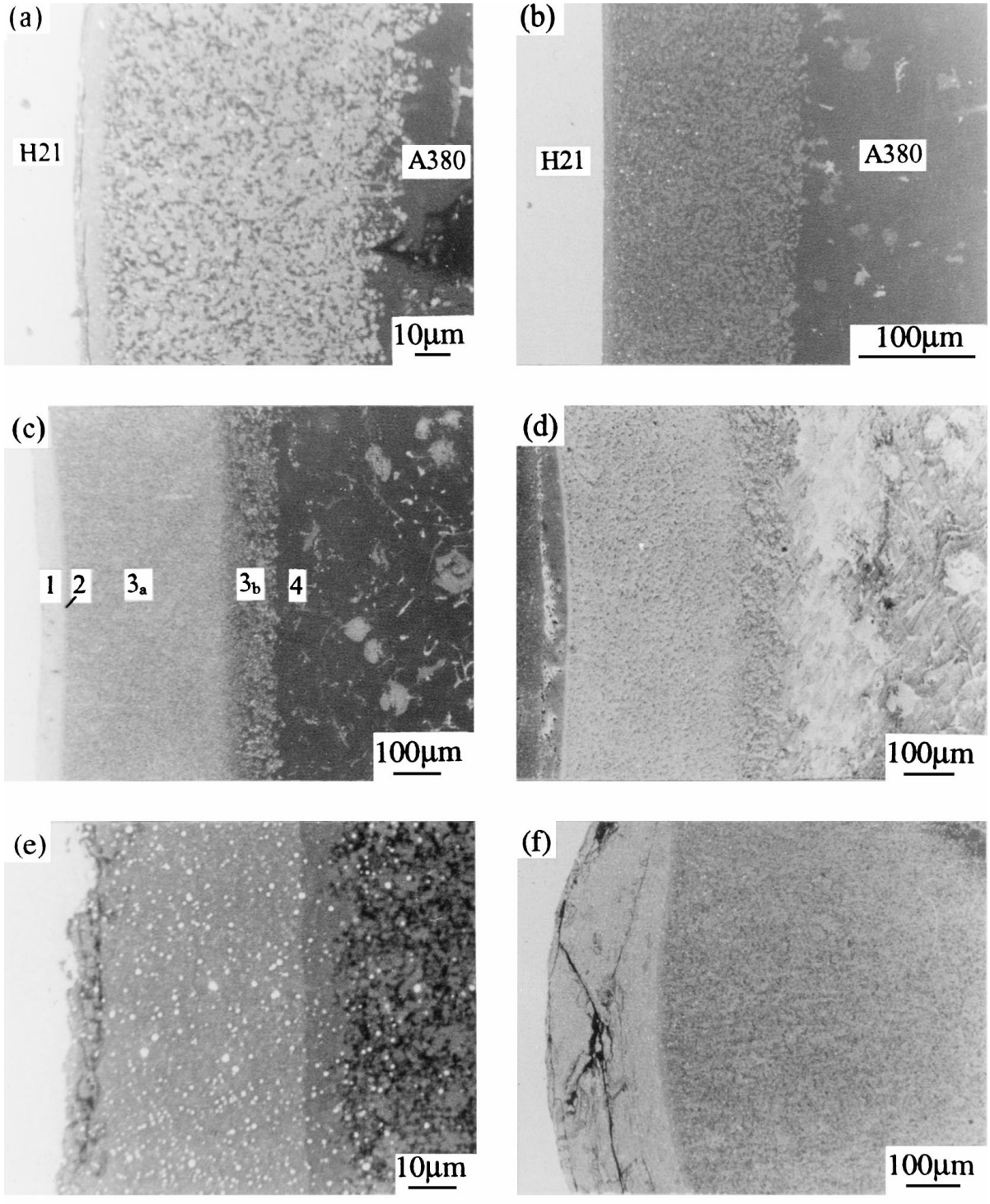

Figure 2 The morphology of the reaction zone between H21 steel and molten A380 alloy after different erosion time. (a) 1 hour; (b) 4 hours; (c), (d) and (e) 9 hours; (f) 16 hours. (d) is a secondary electron image and others are backscattered electron images. In all the SEM micrographs, H21 steel is located at the left-hand side and A380 alloy at the right-hand side.

With the dissolution of intermetallic compounds into liquid aluminium alloy, aluminium melt surrounding the test sample became more and more saturated with iron and other alloying elements of H21 steel. Consequently, $FeAl_3$ phase segregated along the grain boundaries of aluminium alloy close to reaction zone. This was shown in Fig. 3.

The radius decrease of H21 sample, Δr, was plotted in Fig. 4 against the square root of the test time. The average erosion rate was 73 μm per hour in the first 16 hours under the experimental conditions. Δr increases approximately linearly with the increase of the square root of test time, indicating that the erosion was primarily dominated by diffusion. It should be emphasised that unlike most of other investigated materials, the attack depth was not very uniform throughout the periphery of H21 samples. After long-term test like 9 or 16 h the cross-section of samples was not very round. Regions attacked more severely by molten Al-alloy always covered by a thinner reaction zone.

TABLE II Summary of the thickness of interfacial compounds and radius decrease of H21 samples

Test time (hour)	$FeAl_2$ layer (μm)	Fe_2Al_5 layer (μm)	$FeAl_3$ layer (μm)	Decrease in radius (mm)
1	0	8–10	118–123	0.27
4	0	8–10	135–148	0.67
9	20–49	8–10	194–412	0.99
16	80–160	7–10	458–960	1.17

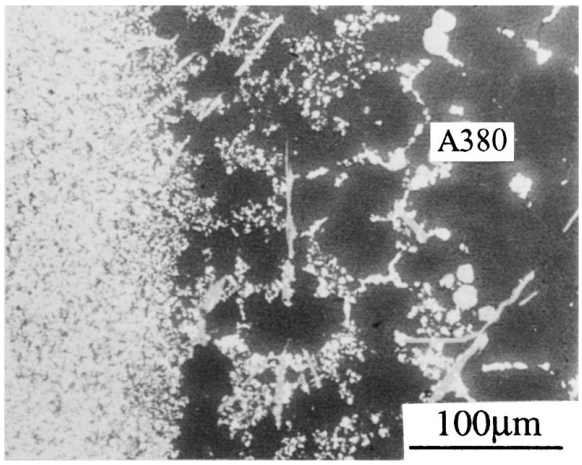

Figure 3 SEM micrograph showing $FeAl_3$ compound precipitated at the grain boundaries of A380 alloy close to the reaction zone between H21 steel and A380 alloy after 16-hour test.

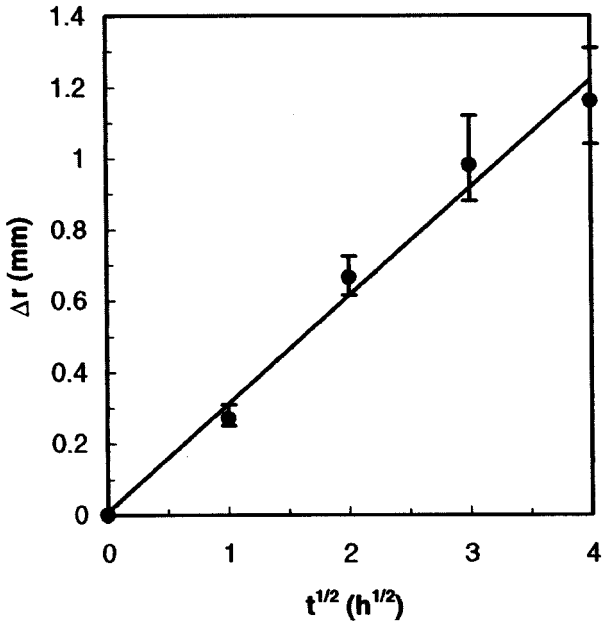

Figure 4 Radius decrease of H21 samples, Δr, plotted against the square root of test time.

EDS line profiles of iron, tungsten, chromium, manganese, aluminium, silicon and copper at the reaction zone after 9-hour test were presented in Fig. 5. Nearly all the major constituent elements of both H21 steel and A380 alloy were present in the reaction zone. This was in agreement with the previous experimental result that the dissolution of alloy elements in steel was uniform, in which all elements in steel diffused into reaction zone in the same ratio as they presented in the steel [10]. Fig. 5

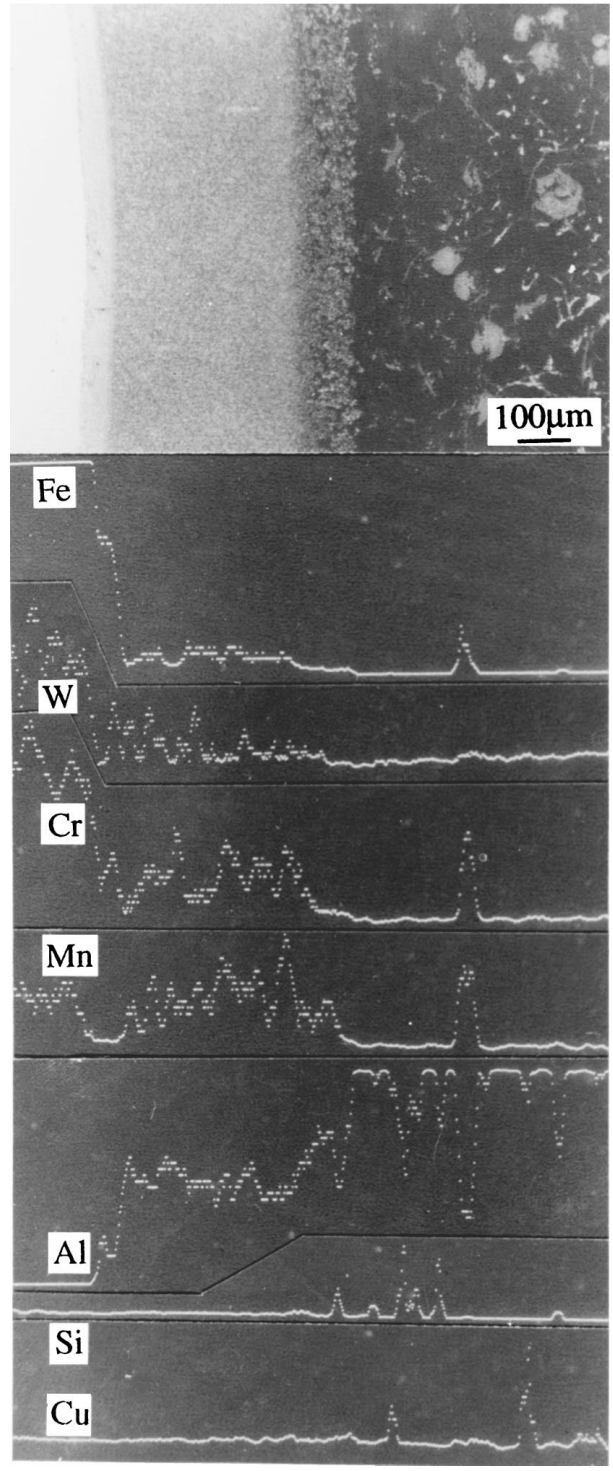

Figure 5 EDS line profiles of the major constituent elements of both H21 and molten 380 at the reaction zone after 9-hour test.

revealed that $FeAl_2$ and Fe_2Al_5 layers were comparatively depleted of tungsten, chromium and manganese. This was also confirmed by spot analyses of different compounds. EDS spot analyses of chemical composition also revealed that the contents of silicon in Fe_2Al_5 and $FeAl_3$ layers were higher than that in $FeAl_2$ layer, while copper contents in all compounds were very low.

The microhardness measurement at the reaction zone after 9-hour test was illustrated in Fig. 6. Since Fe_2Al_5 layer is too thin, it was impossible to measure its microhardness. In $FeAl_2$, $FeAl_3$ and H21 steel, the hardness was quite uniform, having mean values of HV974,

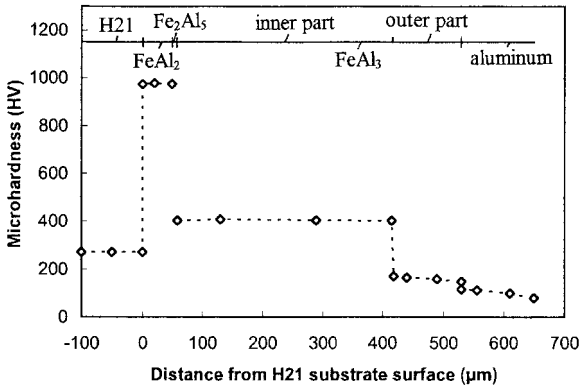

Figure 6 Microhardness profile of the reaction zone between H21 steel and molten A380 alloy after 9-hour test.

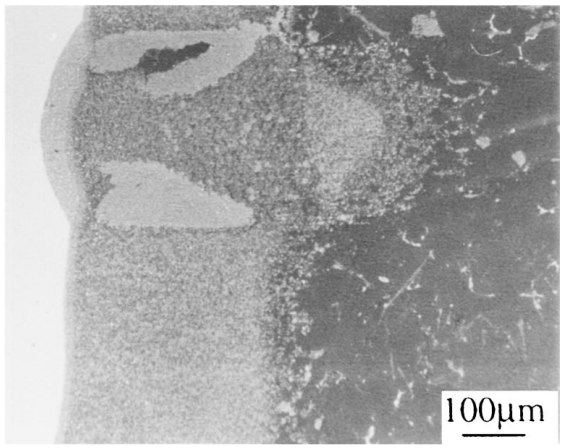

Figure 7 SEM micrograph showing the morphology of the cracked reaction zone between H21 steel and molten A380 alloy after 9-hour test.

HV403 and HV271, respectively. Due to the variation of porosity level, the microhardness of $FeAl_3$ layer showed a decreasing trend towards Al-alloy. Comparison of the measured data with values available in the literature [4, 7, 10] confirmed the phase characterisation results by EDS analysis.

It is well-known that Fe-Al intermetallic compounds are brittle. Due to their brittleness, cracks formed readily within the reaction zone. As shown in Fig. 7, when the reaction zone was cracked, molten aluminium penetrated into the reaction zone, making the underlying H21 steel more deeply attacked.

3.2. Coated samples

The morphology of the reaction zone between Cr_2O_3-coated H21 steel and A380 alloy after 16-hour test was shown in Fig. 8. There was no reaction product observed at the coating-A380 interface. The interface of coating with aluminium kept very straight throughout the test until it was totally removed. Due to the attack from aluminium melt, the coating thickness decreased with time. Under the experimental conditions, after 36-hour test the Cr_2O_3-coating on H21 steel was completely removed. The average decrease of coating thickness, ΔT, is plotted in Fig. 9 against the square root of test time.

From EDS line profiles of aluminium and iron it was found that the diffusion of aluminium and iron through

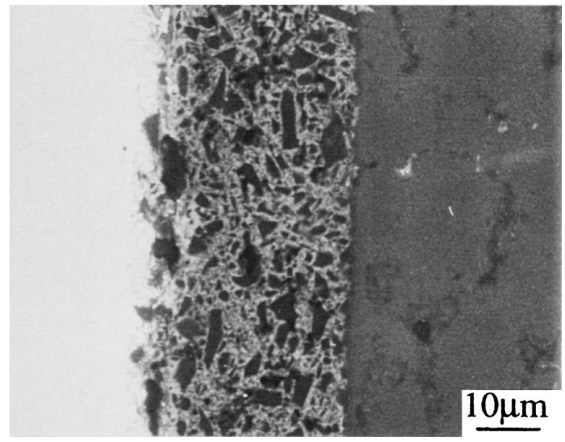

Figure 8 SEM micrograph showing the morphology of the reaction zone between Cr_2O_3-coated H21 steel and molten A380 alloy after 9-hour test.

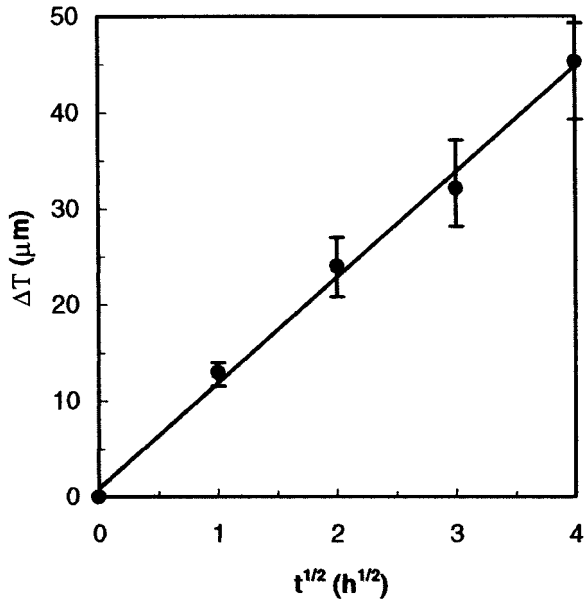

Figure 9 The average decrease in thickness of Cr_2O_3-coating, ΔT, plotted against the square root of test time.

the coating could occur to some extent. Aluminium was detected at the interface of H21-coating and iron was detected at the coating-A380 interface.

4. Discussion

4.1. The nature of reaction zone

Microstructural observation revealed that Fe_2Al_5 and $FeAl_3$ compounds first formed at the interface after 1 hour test. After several hours $FeAl_2$ compound also formed. The successive layers of intermetallic compounds formed between H21 steel and A380 alloy is in agreement with the previous studies on steel and liquid aluminium alloys. The formation of aluminium-rich Al-Fe compounds, Fe_2Al_5 and $FeAl_3$, can be related to the greater interdiffusion coefficients in those compounds compared with iron-rich Al-Fe compounds [10]. The reason for the formation of a thick $FeAl_3$ layer and a thin Fe_2Al_5 layers in H21-A380 reaction zone can be attributed to the high porosity level in $FeAl_3$ phase. Liquid aluminium can directly interact with Fe_2Al_5 compound at Fe_2Al_5-$FeAl_3$ interface, and aluminium melt in this porous layer acts as a fast diffusion path. Therefore, in

this diffusion-controlled process the growth of $FeAl_3$ compound can be accelerated, giving rise to a thick layer.

The thickness of Fe_2Al_5 phase depends on dynamic equilibrium of its growth and consuming rates at both sides of the layer. On one hand, the growth of Fe_2Al_5 phase into steel or $FeAl_2$ phase is primarily dominated by aluminium diffusion to the interface through Fe_2Al_5 phase itself. The growth rate can be relatively slow since Fe_2Al_5 phase is compact. On the other hand, the consumption of Fe_2Al_5 phase by the growing $FeAl_3$ phase can be quick owing to the direct contact of Fe_2Al_5 phase with liquid aluminium through the porous layer. The rough Fe_2Al_5-$FeAl_3$ interface in Fig. 2e is resulted from the different local reaction rates of Fe_2Al_5 phase. It will have a higher consumption rate when it is in contact with liquid aluminium, and a lower consumption rate when in contact with $FeAl_3$ phase.

The presence of alloying elements in the reaction zone might be another important factor for the formation of a thin and stable Fe_2Al_5 layer. Alloying additions, particularly silicon, nickel, and copper, were found to reduce the intermetallic layer thickness. Among them silicon is deemed a most important element [11–13]. Silicon atoms are assumed to occupy the structural vacancies of Fe_2Al_5 phase [6, 14, 15]. Some authors claimed Al-Fe-Si compounds may form, growing more slowly than Fe_2Al_5 [5, 6, 16]. Following those arguments, the reason why Fe_2Al_5 layer did not grew thick steadily in our work may be explained by the high silicon content in A380 melt and high concentration of alloying elements in H21. However, very thin Fe_2Al_5 layer was also reported in the cases of pure aluminium [8, 10]. Therefore, it seems that the dynamic equilibrium between the growth and consuming rates of the Fe_2Al_5 phase is the major mechanism for the formation of a thin and stable Fe_2Al_5 layer.

The observed morphology of intermetallic compounds in this investigation is quite different from that reported in the literature. In the cases of pure solid iron and liquid aluminium, Fe_2Al_5 layer was thick, forming a tongue-like morphology, while a thin $FeAl_3$ layer formed neighbouring liquid aluminium [5, 6, 8]. It was deemed that the growth direction of Fe_2Al_5 coincided with the direction of the c axis of orthorhombic cells was the reason why Fe_2Al_5 grew rapidly and formed tongue-like morphology [3]. However, in the cases of alloy steels or liquid aluminium alloys, the morphology and thickness of intermetallic compounds had a great deal variation, and porosity was sometimes observed [2, 6–12]. It is found that in all cases when a $FeAl_3$ layer was thick it was porous, while when this layer was thin it was compact.

4.2. Effect of dynamic conditions

It is known that liquid agitation affects drastically the solid dissolution process. The dissolution of a solid metal in a liquid metal can be described by the following equation [10, 17]

$$\ln\left(\frac{c_s - c_o}{c_s - c}\right) = k\frac{St}{v} \tag{1}$$

Where c is the concentration of the solute element in the melt, c_s the saturation concentration, c_o the initial concentration of the solute; k the dissolution rate constant, S the surface area of solid metal, v the melt volume, t the time. According to Kassner equation [18], the dissolution rate constant, k, may be expressed as

$$k = 0.554 I^{-1} D^{2/3} \eta^{-1/6} \omega^{1/2} \tag{2}$$

Here ω is the angular rotating speed of the solid metal, η the kinematic viscosity of the melt, D the diffusion coefficient of alloying element across the interfacial zone and I is a function of Schmidt number. According Equation (2), increasing ω will increase the value of k, accordingly increase the value of c. It means that the rapid sample rotation can accelerate the dissolution of compounds, and consequently increase the erosion rate.

In related erosion tests of steels in liquid aluminium alloys, it was confirmed that a large number of protuberances formed at the interfaces of steels with aluminium alloys [7–9]. Those investigations were conducted under either stationary chemical interaction or low rotating velocity of steel sample in liquid aluminium. The protuberances were cylindrical at the base and topped by a cone, growing from reaction zone into aluminium melt. They presented over a temperature range, resulted from the dendritic growth of iron aluminides. However, under our experimental conditions, a planar interface was observed. It is believed that the formation of such planar interface can be attributed to the rapid washing of aluminium melt to the samples. In other words, the shear stresses at the interfacial region can lead to a continuous breaking-off of any convexes, restraining its further growth into protuberances.

4.3. Protective effect of the reaction zone

The high fraction of porosity in $FeAl_3$ layer is detrimental to the erosion resistance of H21 steel in molten Al-alloy. Porosity not only decreases microhardness of $FeAl_3$ layer, making the layer more vulnerable under compressive stress, but also facilitates the diffusion of aluminium and other elements through $FeAl_3$ layer. So, although the thickness of $FeAl_3$ layer is great, its effect on the restraint of diffusion is very poor. In other words, the thick $FeAl_3$ layer can not protect effectively the H21 sample from both mechanical wear and chemical corrosion.

Fe_2Al_5 layer is compact, but since it is very thin (less than 10 μm) its effect on the restraint of diffusion is also limited. In contrast, $FeAl_2$ compound is compact and is well adhered to steel substrate (see Fig. 2b to e). Thus the continuously growing layer can slow down diffusion more effectively than other intermetallic compounds. As a result, after the formation of a thick $FeAl_2$ layer, the erosion rate is decreased as shown in Fig. 6.

Another reason for the declining erosion rate in Fig. 6 is that the diameter of H21 sample decreases with time. Thus with the proceeding of the test there is less sample area available for erosion. With the decrease of sample diameter the tangential velocity at sample periphery is

also decreased. This will in turn decrease the erosion rate.

4.4. Effect of Cr_2O_3 coating

Protective coating is a well-known method to extend the service life of alloys in aggressive environment. It has been demonstrated that Cr_2O_3-coating can substantially restrain the dissolution of H21 steel into molten Al-alloy. However, under the experimental conditions it was found that Cr_2O_3-coating could not survive the long-term test. Since the interface between Cr_2O_3-coating and A380 was straight during the test, and there was no reaction product detected, the deduction of coating thickness with test time (Fig. 9) must be due to chemical dissolution. Aluminium oxide is always present in molten Al-alloy, which can possibly combine with Cr_2O_3 to form complex compounds with a low melting point. Consequently, Cr_2O_3-coating can only act as a diffusion barrier and is not an ideal coating to prevent H21 steel from the chemical attack of molten aluminium.

5. Conclusions

1. $FeAl_3$, Fe_2Al_5 and $FeAl_2$ intermetallic compounds formed in sequence from A380 alloy to H21 steel during the erosion tests performed at 700°C under dynamic conditions. Fe_2Al_5 and $FeAl_2$ compounds were compact, while $FeAl_3$ compound was porous. The thickness of $FeAl_3$ and $FeAl_2$ compounds increased with test time. However, the thickness of Fe_2Al_5 layer kept relatively constant in the range of 7–10 μm.

2. At 700°C the average erosion rate of 10 mm diameter H21 sample rotating at 300 rpm in molten A380 alloy was 73 μm per hour in the first 16-hour test. The high erosion rate can be attributed to the combination of steel dissolution, swift melt agitation and poor protective effect of interfacial layers.

3. The thickness of Cr_2O_3-coating decreased with the increasing test time. Cr_2O_3-coating can only act as a diffusion barrier and is not a ideal coating to prevent H21 steel from the chemical attack of molten aluminium.

Acknowledgements

The authors would like to thank Professor M J Bevis for his useful discussions. Financial support from both EPSRC and Ford Motor Co is acknowledged gratefully.

References

1. H. BERNS, Proc. Inter. Conf. on Tool Materials for Molds and Dies, Illinois, 1987, 45.
2. N. KOMATSU, M. NAKAMURA and H. FUJITA, *J. Inst. Light Metals* **18** (1968) 474.
3. TH. HEUMANN and S. DITTRICH, *Z. Metallkde* **50** (1959) 617.
4. PH. VAILLANT and J. P. PETITET, *J. Mater. Sci.* **30** (1995) 4659.
5. V. N. YEREMENKO, YA. V. NATANZON and V. I. DYBKOV, *ibid.* **16** (1981) 1748.
6. G. EGGELER, W. AUER and H. KAESCHE, *ibid.* **21** (1986) 3348.
7. M. SUNDQVIST and S. HOGMARK, *Tribology Inter.* **26** (1993) 129.
8. F. BARBIER, D. MANUELLI and K. BOUCHE, *Scripta Mater.* **36** (1997) 425.
9. A. W. BATCHELOR, N. P. HUNG and T. K. LEE, *Tribology Inter.* **29** (1996) 41.
10. V. I. DYBKOV, *J. Mater. Sci.* **25** (1990) 3615.
11. S. G. DENNER, R. D. JONES and R. J. THOMAS, *Iron and Steel Inter.* (1975) 241.
12. M. NIINOMI and Y. UEDA, *Trans. Jap. Inst. Met.* **23** (1982) 709.
13. B. GIEREK, *Bulletin Swedish Corrosion Institute* **77** (1977) 1.
14. J. E. NICHOLLS, *Corr. Technol.* **11** (1964) 16.
15. T. HEUMANN and S. DITTRICH, *Z. Metallkde.* **50** (1959) 617.
16. D. I. LAINER and A. K. KURAKIN, *Fiz. Met. Metallov.* **18** (1964) 145.
17. L. L. BIRCUMSHAW and A. C. RIDDIFORD, *Quart. Rev.* **6** (1952) 157.
18. T. F. KASSNER, *J. Electrochem. Soc.* **114** (1967) 689.

Received 9 February
and accepted 25 August 1999